OPEN ACCESS
Journal of Innovative Optical Health Sciences
Vol. 15, No. 5 (2022) 2250026 (12 pages)

DOI: 10.1142/S1793545822500262

World Scientific
www.worldscientific.com

H_2O_2-sensitive nanoscale coordination polymers for photoacoustic tumors imaging via *in vivo* chromogenic assay

Jiayue Zhao*, Fei Gong*,‡,¶, Nailin Yang*, Huali Lei*, Zhihui Han*, Yuqi Yang* and Liang Cheng*,†,§,¶

*Jiangsu Key Laboratory for Carbon-Based Functional Materials and Devices
Institute of Functional Nano & Soft Materials (FUNSOM)
Soochow University, Suzhou 215123 Jiangsu, P. R. China

†Wuhan National Laboratory for Optoelectronics and School of Optical and Electronic Information
Huazhong University of Science and Technology
Wuhan 430074, P. R. China
‡gongfei@suda.edu.cn
§lcheng2@suda.edu.cn

Received 19 March 2022
Accepted 13 April 2022
Published 7 September 2022

Photoacoustic (PA) imaging with much deeper tissue penetration and better spatial resolution had been widely employed for the prevention and diagnosis of many diseases. In this study, a new type of hydrogen peroxide (H_2O_2)-activated photoacoustic nanoprobe [Mn-AH nanoscale coordination polymer nanodots (NCPs)] was successfully synthesized by a simple one-step method in water phase containing 2,2′-azino-bis(3-ethylbenzothiazoline-6-sulfonic acid) (ABTS), horse radish peroxidase (HRP), and manganese ion (Mn^{2+}). After modification by polyethylene glycol (PEG), Mn-AH NCPs exhibited excellent stability and biocompatibility for *in vivo* H_2O_2-responsive chromogenic assay with great specificity and sensitivity. In the presence of H_2O_2, colorless ABTS would be converted by HRP into the oxidized form with strong near-infrared (NIR) absorbance, enabling photoacoustic detection of endogenous H_2O_2. Using H_2O_2-activated Mn-AH NCPs, we have successfully performed PA imaging and H_2O_2 detection of subcutaneous murine colon CT26 tumor and deep-seated orthotopic bladder tumor. Due to the inherent Mn element existence inside the Mn-AH, this nanoprobe also serves as a good T1-weighted magnetic resonance imaging (MRI) contrast agent simultaneously. Lastly, after accomplishing its imaging

¶Corresponding authors.

functions, the Mn-AH NCPs could be cleared out from the body without any long-term toxicity, providing a new opportunity for cancer diagnosis and treatment.

Keywords: Nanoscale coordination polymers (NCPs); PA imaging; MRI; H_2O_2 detection; metabolic nanoprobes.

1. Introduction

As one of the most common reactive oxygen species (ROSs), hydrogen peroxide (H_2O_2) has attracted much attention in many fields such as food production, the textile industry, biological safety, chemical synthesis, and even in many oxidative biological reactions.[1,2] In addition, H_2O_2 plays an important role in cell growth and proliferation.[3] Moderate H_2O_2 is essential for life, but H_2O_2 overexpression may be a signal of disease such as inflammation, infection, diabetes mellitus, and cancers.[4,5] Therefore, the early detection of abnormal levels H_2O_2 will be of great significance in the disease's diagnosis and treatment. For example, tumors are the most lethal disease in the world nowadays and they have much more H_2O_2 ($\sim 100\,\mu$M) than normal tissues.[6,7] It is difficult to effectively treat them when the patients find themselves with tumors in the later period, thus the early detection is very important for the tumor treatment. Up to now, various methods have been developed for the ultra-high sensitive detection of

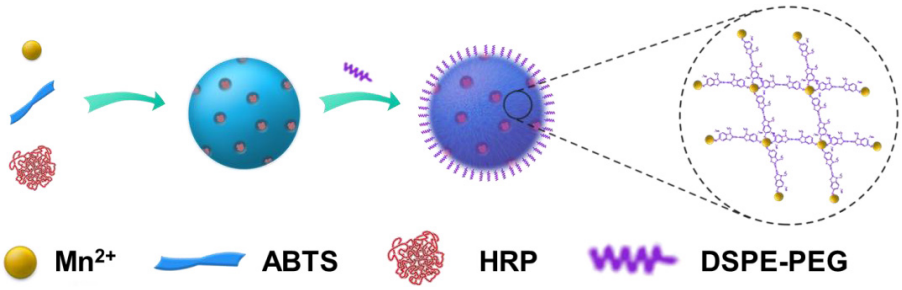

(a)

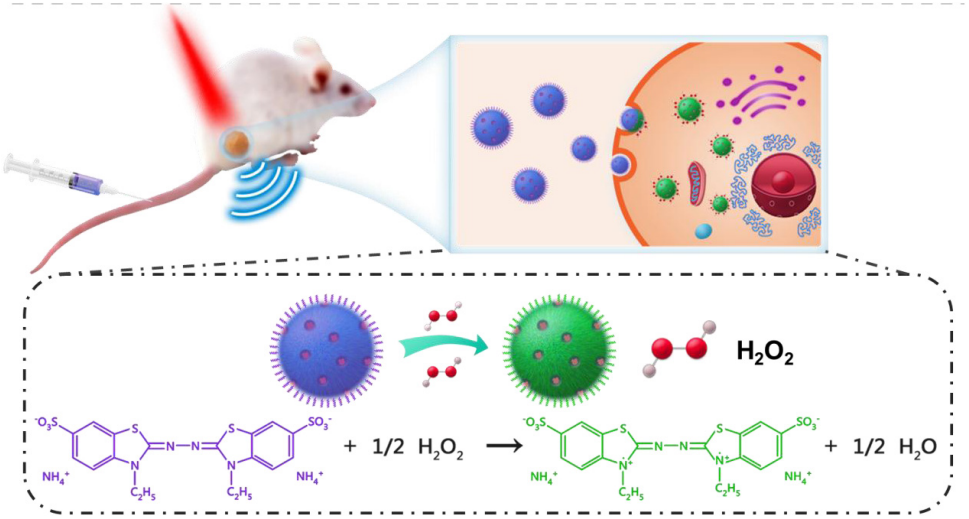

(b)

Scheme 1. Schematic illustration to show the preparation of Mn-AH nanoprobe and their applications for PA tumor imaging. (a) The preparation of Mn-AH NCPs via simple one-step method in water phase containing ABTS, HRP, and Mn^{2+}. (b) *In vivo* PA imaging of murine tumor based on H_2O_2-activated the conversion of ABTS into ABTS$\bullet^+$.

H_2O_2, including chemiluminescence, titrimetry, bioluminescence, and fluorescence.[8,9] However, most of them focused on *in vitro* detection, and the limited tissue penetration depth would hamper *in vivo* H_2O_2 detection. Therefore, there is a great urge to develop new types of method to realize H_2O_2 detection in deep tissue with high specificity and sensitivity.

In recent years, photoacoustic (PA) imaging has attracted increasing attention because of its excellent performance, reasonable penetration depth, highly spatial resolution, noninvasive, and harmless to organisms.[7,10,11] PA imaging uses materials with near infrared (NIR) absorption to generate thermal expansion after absorbing pulsed laser, resulting in the generation of the ultrasound wave. A large variety of organic molecules, with absorption in the NIR "tissue transparent" optical window have been extensively explored as PA imaging probes.[12–16] Although this organic molecules-based PA detection of tumors *in vivo* has been studied, the organic molecules are prone to degradation and quenching under laser irradiation in the detection process, leading to the decrease of detection sensitivity.[17,18] Inorganic nanoprobes have been widely developed recently, but most of them are difficult to degrade in the body for a long-term, affecting their long-term biosafety.[19,20] Therefore, there is a great urge to develop stable and sensitive photoacoustic nanoprobes with good biological safety.

Recently, nanoscale metal–organic coordination polymers (NCPs), due to the properties of the diversity of structural and chemicals, high loading capacity, biodegradability, and excretion from the body, have been widely used in nanomedicine, especially in the field of nano-sized biomedicine for carrying enzyme and gene, imaging molecule, and therapeutic drugs.[21–23] Herein, a new type of Mn-AH NCPs probes was synthesized for *in vivo* PA imaging and detection of molecule H_2O_2 (Scheme 1). According to simple one-step reaction, uniform Mn-ABTS-HRP NCPs were synthesized by mixing Mn^{2+} (metal ion center), ABTS [2,2′-azino-bis (3-ethylbenzothiazoline-6-sulfonic acid), organic framework and HRP substrate], and HRP enzyme catalyst. After that, polyethylene glycol (PEG) was employed to modify them and the final PEGylated Mn-AH NCPs showed high stability and biocompatibility for future *in vivo* application. In the presence of H_2O_2, colorless ABTS would be converted by HRP into the oxidized form with strong NIR absorbance, enabling PA detection of endogenous H_2O_2 with great specificity and sensitivity. Using H_2O_2-activated Mn-AH nanoprobes, we have successfully performed PA imaging and H_2O_2 detection of subcutaneous CT26 colon tumor and deep-seated orthotopic bladder tumor. Due to the inherent Mn element existence inside Mn-AH, this nanoprobe also was served as a good T1-weighted magnetic resonance imaging (MRI) contrast agent simultaneously. Lastly, after accomplishing its imaging functions, Mn-AH NCPs could be cleared out from the body without any long-term toxicity, providing a new opportunity for cancer diagnosis and treatment.

2. Experimental Section

2.1. *Materials*

All chemicals were purchased from Sigma–Aldrich unless specified. ABTS (2,2′-azino-bis(3-ethylbenzothiazoline-6-sulfonic acid)) was purchased from Roche. Horse radish peroxidase (HRP) and manganese chloride ($MnCl_2$) were purchased from Aladdin. DSPE-PEG-5k (1,2-distearoyl-sn-glycero-3-phosphoethanolamine-*N*-(methoxy (polyethylene glycol)-5000)) and hydrogen peroxide (H_2O_2) were purchased from Laysan Bio Inc. and China National Pharmaceutical Group Corporation, respectively. The water used in the experiment is deionized water.

2.2. *Preparation of Mn-ABTS-HRP-PEG (Mn-AH)*

We developed a simple method to synthesize Mn-AH NCPs. First, 9 mg ABTS, 2 mg HRP, 9 mg $MnCl_2$, and 1.5 mL water were added to the serum bottle and stirring 1 h. Then, centrifuged the aqueous solution to obtain Mn-ABTS-HRP product and then dissolve the product in 1 mL water for further modification. Finally, 10 mg DSPE-PEG was added to the above 1 mL aqueous solution for stirring 1 h, and concentrated the mixed solution by ultrafiltration to gain Mn-ABTS-HRP-PEG. As determined by BCA, UV–Vis absorbance, and ICP-OES analysis, the concentration of ABTS, HRP, and Mn^{2+} inside the Mn-AH nanoprobe were quantified.

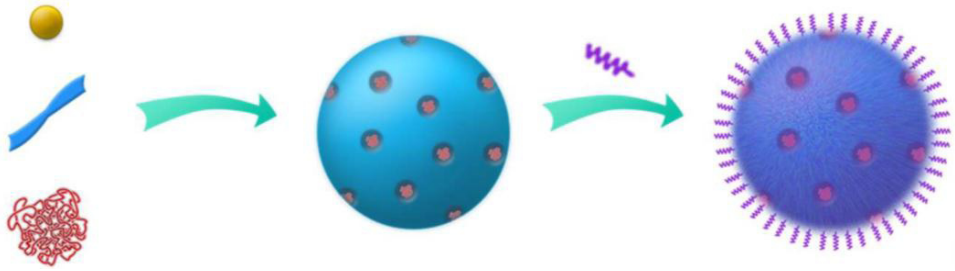

(a)

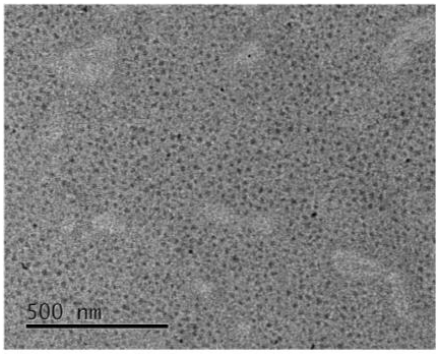

(b)

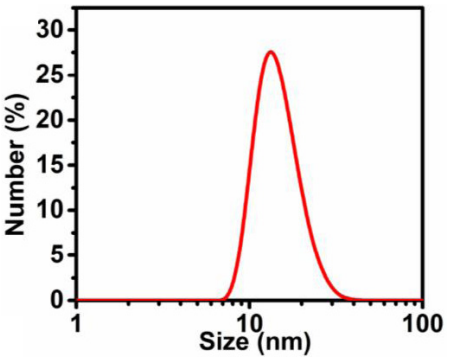

(c)

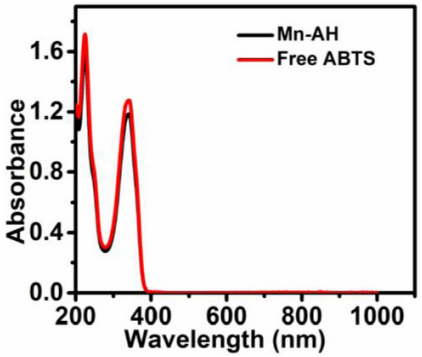

(d)

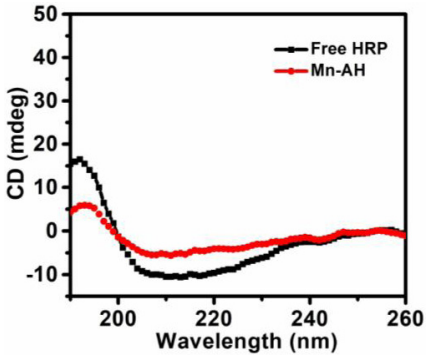

(e)

Fig. 1. Synthesis and characterization of Mn-AH nanoparticles. (a) Schematic illustration to show the fabrication process of Mn-AH nanoparticles. ((b), (c)) TEM image (b) and DLS (c) of Mn-AH. (d) UV–Vis spectra of Mn-AH and free ABTS dye. (e) CD spectra of Mn-AH and free HRP enzyme.

2.3. *Characterization of Mn-AH NCPs*

Transmission electron microscope (TEM) imaging and elemental mapping were carried out by a FEI Tecnai F20 TEM. Dynamic light scattering (DLS) was measured using a Zetasizer Nano Z (Malvern). UV–Vis–NIR absorbance spectra were recorded by PerkinElmer Lambda 750 UV–Vis–NIR spectrophotometer. The PA imaging was carried out by a photoacoustic computerized tomography scanner (in Vision 256, iThera Medical), while the PA imaging of animals was conducted by a Vevo LAZR Imaging System (FujiFilm VisualSonics Inc.).

2.4. *Sensitivity of Mn-AH nanoprobes*

To study the sensitivity of Mn-AH nanoprobe for H_2O_2 detection, different concentrations of H_2O_2 (0.5–100 μM) were incubated with Mn-AH nanoprobe, and the absorption of the solutions at 800 nm was determined by UV–Vis absorbance spectra. In

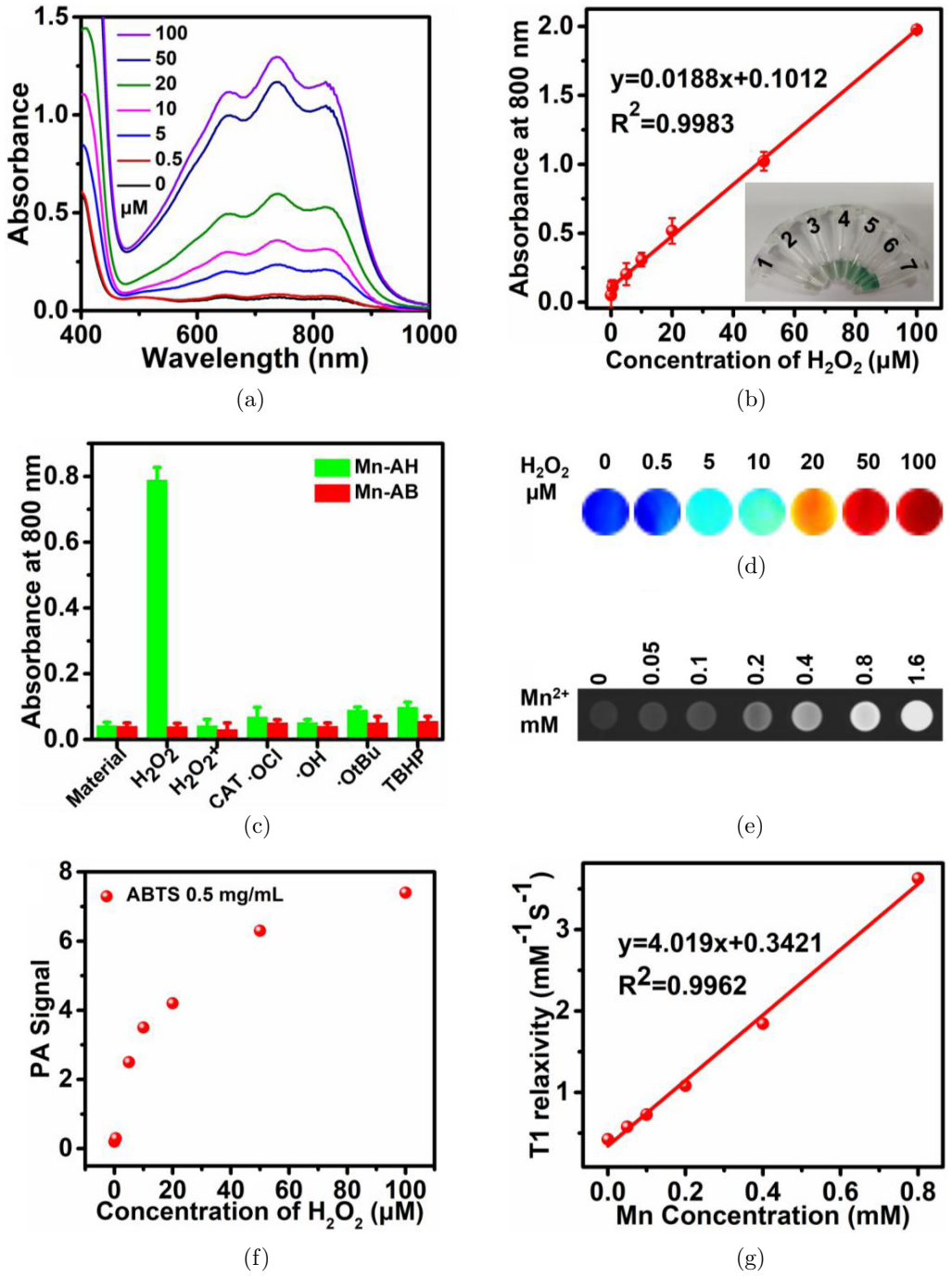

Fig. 2. Mn-AH nanoprobe for H_2O_2-activated PA imaging and MRI. (a, b) UV–Vis absorbance spectra (a) and absorbance at 800 nm (b) of Mn-AH after incubated with various concentrations of H_2O_2 (0–100 μM). (c) Absorbance of Mn-AH and Mn-AB at 800 nm after incubation with various types of ROS as indicated. ((d), (f)) PA images (d) and PA signal intensities (f) of Mn-AH dispersed in buffer with different H_2O_2 concentrations. ((e), (g)) MRI (e) and T1 relaxation rates (g) of various concentration of Mn-AH.

addition, PA imaging of Mn-AH after incubation with H_2O_2 was carried out by a photoacoustic computerized tomography scanner (in Vision 256, iThera Medical).

2.5. *Specificity of Mn-AH nanoprobes*

To study the specificity in the detection of H_2O_2, Mn-AH NCPs were incubated with various kinds of ROS (25 μM) for 20 min. H_2O_2, TBHP, and $^{-}$OCl were

prepared by dilution from stock solutions obtained from China National Pharmaceutical Group Corporation. •OH and •OtBu were generated by reaction of 1 mM $FeCl_2$ with 25 μM H_2O_2 or TBHP, respectively. O_2^- was delivered from a 10 mM stock solution of potassium superoxide (KO_2) in DMSO. Then, the absorbance of Mn-AH solution at 800 nm after incubated with each ROS was measured.

2.6. *Tumor models*

Balb/c or nude mice were obtained from Changzhou Qiawensi Experimental Animals Co. Ltd., and all the animal experiments were carried out under the protocols approved by Soochow University Laboratory Animal Center.

To obtain the subcutaneous tumor model, 10^6 CT26 cells dispersed in 50 μL PBS were subcutaneously injected into the back of each mouse. When the tumor size reached $\sim 100\,mm^3$, Mn-AH NCPs were intratumorally or intravenously injected into the mice bearing CT26 tumor.

To obtain the orthotopic bladder cancer (OBC) tumor model, 10^6 fLuc-T24 cells dispersed in 50 μL PBS were injected into the bladder wall. Then, bioluminescence imaging was conducted to monitor the tumor growth. At 14 days, there nude mice were intravenously injected or intravesical instillation with Mn-AH nanoprobe for future PA imaging.

2.7. *In vivo PA imaging of tumor*

The mice-bearing CT26 tumor was intratumorally or intravenously injected Mn-AH nanoprobe, and then PA imaging was conducted at various time points with a Vevo LAZR imaging system (FujiFilm VisualSonics Inc.). Moreover, the T24-tumor-bearing nude mice were intravenously injected Mn-AH NCPs, and then imaged by PA system.

2.8. *In vivo MRI of tumor*

For MR imaging, different concentrations of Mn-AH NCPs (0–1.6 mM [Mn]) were measured via a 3T clinical MR scanner. CT26 tumor-bearing mice were scanned using the same scanner equipped with a special coil for small-animal imaging before and after i.t. or i.v. injection with Mn-AH NCPs. Axial T1 weighted MRI imaging was performed under the technical parameters including: TR/TE = 400/15; matrix size: 320*192; field of view (FOV) 60*60 mm; thickness/spacing: 3/0.5 mm; gap: 0.2 mm; examination time: 3–5 min.

3. Results and Discussion

3.1. *Synthesis and characterization of Mn-AH NCPs*

In this work, Mn-AH NCPs were synthesized by simple one-step reaction. In brief, a mixture containing ABTS [2,2′-azino-bis(3-ethylbenzothiazoline-6-sulfonic acid)] as organic framework and substrate, horse radish peroxidase (HRP) as catalytic center, and manganese chloride ($MnCl_2$) as central metal was added to the serum bottle and stirred for 1 h to obtain Mn-ABTS-HRP (Fig. 1(a)). As revealed by transmission electron microscopy (TEM) imaging, the Mn-ABTS-HRP nanoscale coordination polymers (Mn-AH NCPs) were successfully formed, and these products showed very uniform morphology with an average diameter of ~ 15 nm (Fig. 1(b)). In order to enhance their physiological stability, the synthesized Mn-ABTS-HRP NCPs were modified by DSPE-PEG (1,2-distearoyl-sn-glycero-3-phosphoethanolamine-*N*-(methoxy (polyethylene glycol)-5000)), and the obtained Mn-ABTS-HRP-PEG NCPs showed excellent stability in water, phosphate buffer saline (PBS), and DMEM culture medium (Figs. 1(c) and S1). The concentration of ABTS, HRP, and Mn^{2+} inside the Mn-AH nanoprobe was determined to be 38.89%, 28%, and 14.4% by UV–Vis absorbance spectra, bicinchoninic acid (BCA) protein assay, and inductively coupled plasma optical emission spectrometry (ICP-OES) (Figs. 1(d) and S2). The thermogravimetric analysis (TGA) also confirmed NCPs structure (Fig. S3). The structure of HRP protein was measured by CD and found the secondary structure of the final NCPs nanoprobes were not destroyed, indicating that the HRP in Mn-AH NCPs still had good catalytic activity (Fig. 1(e)). In order to compare the activity of the enzyme, bull serum albumin (BSA) was used to replace HRP to synthesize Mn-ABTS-BSA-PEG (Mn-AB) NCPs. TEM imaging showed the circular structure of Mn-AB NCP with the size of ~ 30 nm (Fig. S4). From UV–Vis absorbance spectra of the final products, ABTS had been successfully combined into the structure of Mn-AB (Fig. S5).

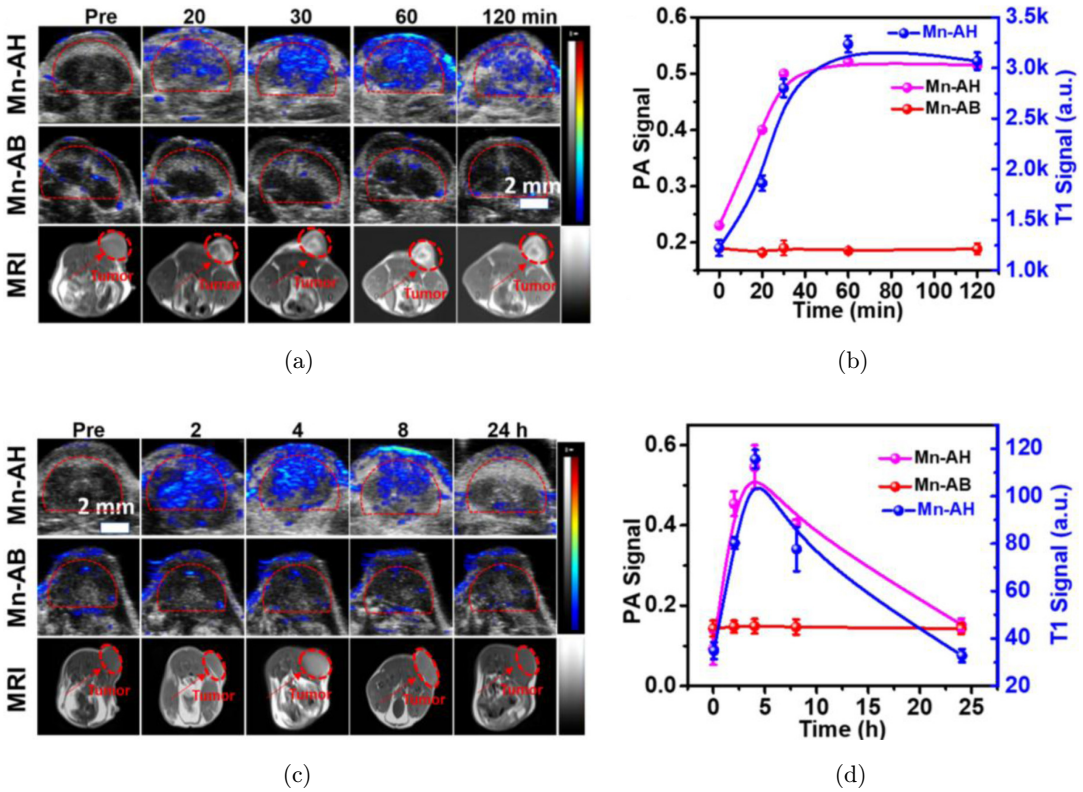

Fig. 3. *In vivo* PA imaging and MRI for CT26 subcutaneous tumor. (a) *In vivo* PA imaging and MRI of CT26 tumor of mice after i.t. injection of Mn-AH (50 μL). (b) PA signal and T1 signals of mouse tumor based on PA imaging and MRI data in a. (c) *In vivo* PA imaging and MRI of CT26 tumor of mice after i.v. injection of Mn-AH (200 μL). (d) PA signal and T1 signal of mouse tumor based on PA imaging and MRI data in a. Mn-AH dose: 3.5 mg/mL ABTS, 0.56 mg/mL HRP, or BSA and 1.3 mg/mL Mn^{2+}.

3.2. *In vitro PA detection of H_2O_2*

HRP has been extensively used in biochemistry applications such as ELISA (enzyme linked immunosorbent assay), owing to its high efficiency to catalyze the conversion of chromogenic substrates such as ABTS into colored products.[24,25] After successfully synthesizing Mn-AH NCPs, we wondered whether this nanoprobe could be used for H_2O_2 detection. As revealed in Fig. 2(a), different concentrations of H_2O_2 (0–100 μM) were incubated with Mn-AH nanoprobe (0.05 mg/mL ABTS). Obviously, after reaction for 20 min, the color of this mixture changed from colorless to distinct green. Meanwhile, the characteristic peak of ABTS at 800 nm was greatly increased with the increasing H_2O_2 concentration. The concentration of H_2O_2 and the absorption at 800 nm was concluded to linear relationship (Fig. 2(b)), and the detection limit of Mn-AH NCPs for H_2O_2 was determined to be $\sim 0.5\,\mu$M. According to the Michaelis–Menten equation,[26] if the H_2O_2 concentration was far below than that of the substrate (ABTS), the ABTS oxidation was catalyzed by HRP in the presence of H_2O_2 by the following reaction:

$$\text{ABTS} + 1/2\text{H}_2\text{O}_2 \quad \rightarrow \text{ABTS}\bullet^+ + 1/2\text{H}_2\text{O},$$

The H_2O_2 specificity of this reaction was evaluated by incubating Mn-AH or Mn-AB NCPs with different types of ROS (25 μM), including H_2O_2, H_2O_2 pretreated with catalase (Cat, 0.2 mg/mL), hypochlorite (•OCl), hydroxyl radical (•OH), *tert*-butoxy radical (•OtBu), and *tert*-butyl hydroperoxide (TBHP). It was found that Mn-AB NCPs showed no appreciable response to all types of ROS. In contrast, Mn-AH NCPs incubated with H_2O_2 showed obviously increased UV–Vis absorbance, whereas there was no significant absorbance change when Mn-AH incubated with H_2O_2 pretreated by Cat to trigger decomposition of H_2O_2, or other types of ROS except for superoxide, which induced a slight response for Mn-AH (Fig. 2(c)), indicating that Mn-AH NCPs could serve as a highly specific probe for detection of H_2O_2 in the physiological environments.

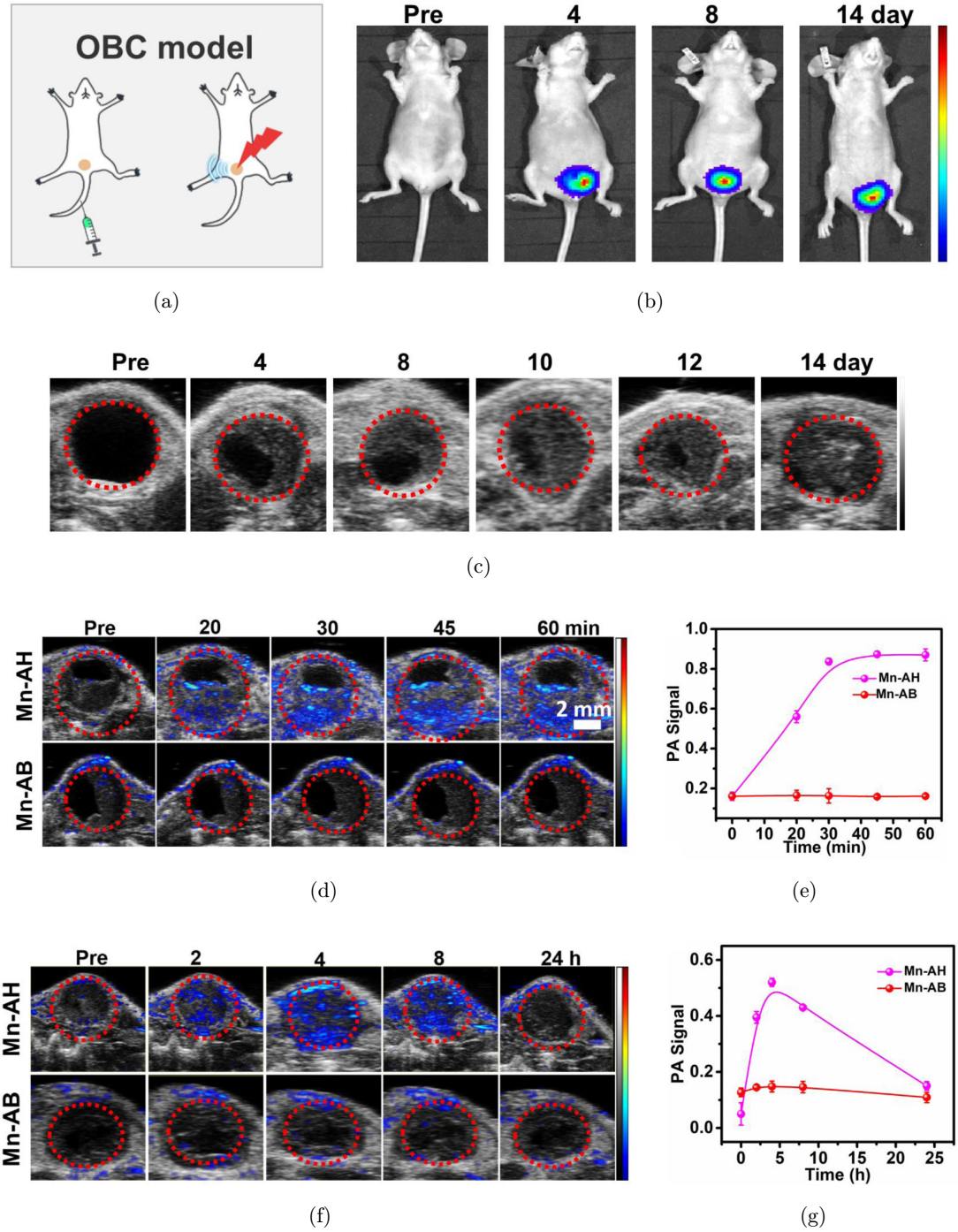

Fig. 4. *In vivo* PA imaging of orthotopic bladder cancer (OBC) model by Mn-AH. (a) Scheme shows the PA imaging of OBC via Mn-AH. ((b), (c)) Bioluminescence (b) and ultrasound (c) imaging to monitor the OBC model growth during 0–14 days. ((d), (f)) PA imaging of OBC tumor of mice by intravesical instillation (d) and i.v. injection (f) of Mn-AH. ((e), (g)) Quantitative analysis of PA signals of OBC tumor based on PA imaging in d and f, respectively.

Since the high absorbance of this nanoprobe reacted with H_2O_2, the synthesized Mn-AH NCPs could be used for PA imaging under the condition of H_2O_2 environment. After reaction of Mn-AH with H_2O_2, ATBS in the structure became oxidized form ABTS$\bullet^+$, which had strong near infrared absorption, therefore, it could realize photoacoustic (PA) imaging detection by OFF-ON model. Then, we

studied the possibility of using PA imaging for H_2O_2 detection based on Mn-AH NCPs. PA imaging of Mn-AH incubated in solutions with different H_2O_2 concentrations showed that as the H_2O_2 concentrations increased the detected PA signals of Mn-AH at 800 nm showed a significant increase (Fig. 2(d)). Notably, for a solution with a rather low concentration of H_2O_2 at 0.5 μM, a substantial level of PA signals could still be detected from Mn-AH, suggesting the great sensitivity of this nanoprobe for PA detection of H_2O_2 down to the submicromolar level (Fig. 2(f)). Therefore, such Mn-AH NCPs could be used for the detection of H_2O_2 with high specificity and sensitivity.

Since Mn^{2+} with five unpaired 3*d* electrons has been demonstrated to serve as a good T1-shortening agent for MR imaging, there is a potential ability of Mn-AH NCPs for enhancing magnetic resonance imaging (MRI).[27,28] Different concentrations of Mn-AH (containing 0–1.6 mM [Mn]) solutions were scanned using an MR scanner. Mn-AH NCPs showed concentration-dependent MR signal enhancement, and the $r1$ relaxivity was calculated to be $\sim 4.02\,mM^{-1}\,s^{-1}$ (Figs. 2(e) and 2(g)), suggesting the feasibility of Mn-AH as novel MR contrast agents. Due to the advantages of PA imaging and MRI with good tissue penetrability and noninvasiveness, the synthesized Mn-AH nanoprobe could be endowed with dual modal diagnostic imaging functionality with high sensitivity and strong spatial resolution.

3.3. *In vivo PA imaging of tumor*

H_2O_2 plays an important role in many physiological processes, thus designing sensitive probes to monitor H_2O_2 levels would be useful for disease diagnosis and treatment.[6,7] Due to the high H_2O_2 level ($\sim 100\,\mu$M) in the tumor microenvironment (TME), *in vivo* PA imaging of endogenous H_2O_2 was first conducted on a subcutaneous murine colon CT26 tumor model. Before conducting animal experiments, the cytotoxicity of Mn-AH NCPs to the cells was first detected. There was no obvious toxicity of Mn-AH NCPs after incubation with different cell lines (murine breast 4T1 cancer cells, murine colon CT26 cancer cells, and human T24 bladder cancer cells), which indicated the good biocompatibility of the Mn-AH NCPs (Fig. S6). Then, *in vivo* PA imaging of tumor was carried out. After intratumoral (i.t.) injection of Mn-AH nanoprobe (50 μL, containing 3.5 mg/mL ABTS, 0.56 mg/mL HRP and 1.3 mg/mL Mn^{2+}), the PA signals of tumor at 800 nm remarkably increased over time and achieved the maximum intensity at 30 min, while the Mn-AB at 800 nm was almost unchanged, demonstrating that our Mn-AH nanoprobe could be activated by the endogenous H_2O_2 inside the tumor (Figs. 3(a) and 3(b)). Next, based on the property that Mn-AH NCPs could be enriched in the tumor by enhanced permeability and retention (EPR) effect after i.v. injection, we conducted the PA imaging of tumor by intravenous (i.v.) injection of Mn-AH nanoprobe (200 μL). Similarly, PA signals of tumor at 800 nm also increased significantly after the probes injection and achieved the maximum at 4 h (Figs. 3(c) and 3(d)). However, the PA signals decrease gradually with prolonging the time, which mainly ascribed to biological decomposition and metabolism of Mn-AH NCPs from the tumor. These results verified the feasibility of Mn-AH NCPs as an efficient H_2O_2-activated probe for PA imaging of tumor. Apart from PA imaging, *in vivo* MRI of tumor was conducted after Mn-AH NCPs injection. Similarly, a notable brightening contrast in the tumor was observed, and the MR signals increased over time and achieved the maximum values at 30 min post i.t. injection of Mn-AH NCPs (Figs. 3(a) and 3(b)). After i.v. injection of Mn-AH NCPs, the tumor presented the most obvious brightening effect at 4 h, and then MR signal decreased (Figs. 3(c) and 3(d)), further confirming that Mn-AH NCPs could be decomposed and excreted from the mice body.

Due to PA imaging with much deeper tissue penetration and better spatial resolution,[29] orthotopic bladder cancer (OBC) tumor model was established to explore the usability of Mn-AH NCPs (Fig. 4(a)). 10^6 fLuc-T24 cells dispersed in 50 μL PBS were injected into the bladder wall to construct the OBC tumor. According to the bioluminescence imaging (Figs. 4(b) and S7), ultrasound imaging (Figs. 4(c) and S8), and H&E-stained tumor slices (Fig. S9), the OBC tumor model on nude mice was successfully constructed. After one week for tumor construction, it was found that the Mn-AH nanoprobe showed unsatisfied PA signal enhancement, which was mainly due to the relatively small tumor size and the lower H_2O_2 concentration (Fig. S10). Thus, after two weeks for tumor growth, Mn-AH NCPs were injected into the murine bladder by intravesical instillation (50 μL,

containing 3.5 mg/mL ABTS, 0.56 mg/mL HRP and 1.3 mg/mL Mn^{2+}). The group of Mn-AH NCPs injection showed significant PA signal in the bladder tumor and achieved the strongest intensity at 45 min (Figs. 4(d) and 4(e)). Meanwhile, we also observed the significant PA enhancement in murine bladder tumor post i.v. injection of Mn-AH NCPs (Figs. 4(f) and 4(g)). However, there was no change in the PA signals in Mn-AB group whether intravesical installation or i.v. injection (Figs. 4(d) and 4(f)). Collectively, our results demonstrated that Mn-AH NCPs could be used for H_2O_2-activated PA imaging in both subcutaneous tumor and deep-seated tumor.

3.4. *In vivo excretion of Mn-AH*

The biodegradability of nanoprobe is very important before biological application.[30,31] Based on the previous PA imaging and MRI, we speculated that Mn-AH NCPs could be decomposed and cleared out from the mice body. Thus, the biodegradable performance and body clearance behaviors of Mn-AH were carefully investigated Mn element determined by ICP-OES. The time-dependent biodistribution showed that significant retention of Mn-AH NCPs was mainly detected in the liver at 24 h time point (Fig. S11(a)). However, the Mn element levels in the main organs rapidly decreased in the following time points (3D and 7D), indicating their good biodegradable performance and body clearable behaviors. The mouse urine and feces were also collected every day to measure Mn levels. Notably, high levels of Mn element were detected in the urine, suggesting that these Mn-AH NCPs would be gradually degraded into ions or ultrasmall nanodots to allow efficient renal excretion (Fig. S11(b)). Considering the efficient biodegradation and clearance, these Mn-AH nanoprobes would not cause significant toxicity to the mouse, promising for their *in vivo* multimodal imaging applications.

4. Conclusions

To conclude, we successfully synthesized Mn-AH NCPs by a simple one-step method in water phase containing HRP (catalytic center), ABTS (HRP substrate and organic framework), and Mn^{2+} (central metals). After modification by DSPE-PEG, Mn-AH NCPs exhibited excellent stability and biocompatibility in physical environment for future *in vivo* imaging. In the presence of H_2O_2, colorless ABTS would be converted by HRP into the oxidized form with strong NIR absorbance, enabling photoacoustic detection of endogenous H_2O_2. Due to the H_2O_2-activated NIR absorbance enhancement and the inherent Mn element existence, the obtained Mn-AH nanoprobe could use for PA/MR dual-modal imaging and *in vivo* H_2O_2 detection. Utilizing the high expression of H_2O_2 in the tumor microenvironment, we successfully imaged subcutaneous CT26 tumor and deep-seated orthotopic tumor based on endogenous H_2O_2-activated PA signal enhancement. In addition, Mn-AH NCPs also could be successfully metabolized from the mouse body after accomplishing its imaging and detection functions. In a word, Mn-AH NCPs with metabolic and biological behavior were used for H_2O_2-activated PA imaging and MRI, providing a new opportunity for the diagnosis and treatment of tumor. Especially, post i.v. injection with the synthesized Mn-AH nanoprobe, we would distinguish the early-stage metastatic tumors from the normal tissues based on H_2O_2-activated PA imaging.

Conflicts of Interest

The authors declare that there are no conflicts of interest relevant to this paper.

Acknowledgments

This article was partially supported by the Innovation Fund of WNLO 2018WNLOKF024, the National Natural Science Foundation of China (U20A20254, 52072253), the China Postdoctoral Science Foundation (2021TQ0229, 2021M702381), Collaborative Innovation Center of Suzhou Nano Science and Technology, the 111 Project, Jiangsu Natural Science Fund for Distinguished Young Scholars (BK20211544), and Suzhou Key Laboratory of Nanotechnology and Biomedicine.

References

1. C. C. Winterbourn, "Reconciling the chemistry and biology of reactive oxygen species," *Nat. Chem. Biol.* **4**, 278–286 (2008).
2. F. Gong, N. Yang, X. Wang, Q. Zhao, Q. Chen, Z. Liu, L. Cheng, "Tumor microenvironment-responsive intelligent nanoplatforms for cancer theranostics," *Nano Today* **32**, 100851 (2020).

3. C. Van de Bittner Genevieve, A. Dubikovskaya Elena, R. Bertozzi Carolyn, J. Chang Christopher, "*In vivo* imaging of hydrogen peroxide production in a murine tumor model with a chemoselective bioluminescent reporter," *Proc. Natl. Acad. Sci. USA* **107**, 21316–21321 (2010).
4. J. Chen, H. Gao, Z. Li, Y. Li, Q. Yuan, "Ferriporphyrin-inspired MOFs as an artificial metalloenzyme for highly sensitive detection of H_2O_2 and glucose," *Chin. Chem. Lett.* **31**, 1398–1401 (2020).
5. H. Kong, C. Fang, Q. Chu, Z. Hu, Y. Fu, G. Han, X. Li, Y. Zhou, "Catalytic core-shell nanoparticles with self-supplied calcium and H_2O_2 to enable combinational tumor inhibition," *J. Nanobiotechnol.* **19**, 313 (2021).
6. F. Gong, N. Yang, Y. Wang, M. Zhuo, Q. Zhao, S. Wang, Y. Li, Z. Liu, Q. Chen, L. Cheng, "Oxygen-deficient bimetallic oxide $FeWO_X$ nanosheets as peroxidase-like nanozyme for sensing cancer via photoacoustic imaging," *Small* **16**, 2003496 (2020).
7. Q. Chen, C. Liang, X. Sun, J. Chen, Z. Yang, H. Zhao, L. Feng, Z. Liu, "H_2O_2-responsive liposomal nanoprobe for photoacoustic inflammation imaging and tumor theranostics via in vivo chromogenic assay," *Proc. Natl. Acad. Sci. USA* **114**, 5343–5348 (2017).
8. L. Yu, Y. Chen, H. Chen, "H_2O_2-responsive theranostic nanomedicine," *Chin. Chem. Lett.* **28**, 1841–1850 (2017).
9. J. Wang, Y. Zhang, E. Archibong, F. S. Ligler, Z. Gu, "Leveraging H_2O_2 levels for biomedical applications," *Adv. Biosyst.* **1**, 1700084 (2017).
10. Q. Tao, G. He, S. Ye, D. Zhang, Z. Zhang, L. Qi, R. Liu, "Mn doped Prussian blue nanoparticles for T1/T2 MR imaging, PA imaging and Fenton reaction enhanced mild temperature photothermal therapy of tumor," *J. Nanobiotechnol.* **20**, 18 (2022).
11. D. Y. Zhang, H. Liu, M. R. Younis, S. Lei, Y. Chen, P. Huang, J. Lin, "*In-situ* TiO_{2-x} decoration of titanium carbide MXene for photo/sono-responsive antitumor theranostics," *J. Nanobiotechnol.* **20**, 53 (2022).
12. Q. Wang, B. Xia, J. Xu, X. Niu, J. Cai, Q. Shen, W. Wang, W. Huang, Q. Fan, "Biocompatible small organic molecule phototheranostics for NIR-II fluorescence/photoacoustic imaging and simultaneous photodynamic/photothermal combination therapy," *Mater. Chem. Front.* **3**, 650–655 (2019).
13. Q. Fu, R. Zhu, J. Song, H. Yang, X. Chen, "Photoacoustic imaging: Contrast agents and their biomedical applications," *Adv. Mater.* **31**, 1805875 (2019).
14. H. Ding, Y. Cai, L. Gao, M. Liang, B. Miao, H. Wu, Y. Liu, N. Xie, A. Tang, K. Fan, X. Yan, G. Nie, "Exosome-like nanozyme vesicles for H_2O_2-responsive catalytic photoacoustic imaging of xenograft nasopharyngeal carcinoma," *Nano Lett.* **19**, 203–209 (2019).
15. W. Yang, X. Shi, Y. Shi, D. Yao, S. Chen, X. Zhou, B. Zhang, "Beyond the roles in biomimetic chemistry: An insight into the intrinsic catalytic activity of an enzyme for tumor-selective phototheranostics," *ACS Nano*, **12**, 12169–12180 (2018).
16. F. Liu, L. Lin, Y. Zhang, Y. Wang, S. Sheng, C. Xu, H. Tian, X. Chen, "A tumor-microenvironment-activated nanozyme-mediated theranostic nanoreactor for imaging-guided combined tumor therapy," *Adv. Mater.* **31**, 1902885 (2019).
17. H. Wang, J. Chang, M. Shi, W. Pan, N. Li, B. Tang, "A dual-targeted organic photothermal agent for enhanced photothermal therapy," *Angew. Chem. Int. Ed.* **58**, 1057–1061 (2019).
18. U. S. Dinish, Z. Song, C. J. H. Ho, G. Balasundaram, A. B. E. Attia, X. Lu, B. Z. Tang, B. Liu, M. Olivo, "Single molecule with dual function on nanogold: Biofunctionalized construct for in vivo photoacoustic imaging and SERS biosensing," *Adv. Funct. Mater.* **25**, 2316–2325 (2015).
19. Q. Miao, K. Pu, "Organic semiconducting agents for deep-tissue molecular imaging: Second near-infrared fluorescence, self-luminescence, and photoacoustics," *Adv. Mater.* **30**, 1801778 (2018).
20. X. Zheng, L. Wang, S. Liu, W. Zhang, F. Liu, Z. Xie, "Nanoparticles of chlorin dimer with enhanced absorbance for photoacoustic imaging and phototherapy," *Adv. Funct. Mater.* **28**, 1706507 (2018).
21. Y. Yang, L. Xu, W. Zhu, L. Feng, J. Liu, Q. Chen, Z. Dong, J. Zhao, Z. Liu, M. Chen, "One-pot synthesis of pH-responsive charge-switchable PEGylated nanoscale coordination polymers for improved cancer therapy," *Biomaterials* **156**, 121–133 (2018).
22. W. Zhu, J. Zhao, Q. Chen, Z. Liu, "Nanoscale metal-organic frameworks and coordination polymers as theranostic platforms for cancer treatment," *Coord. Chem. Rev.* **398**, 113009 (2019).
23. J. Zhao, Y. Yang, X. Han, C. Liang, J. Liu, X. Song, Z. Ge, Z. Liu, "Redox-sensitive nanoscale coordination polymers for drug delivery and cancer theranostics," *ACS Appl. Mater. Interfaces* **9**, 23555–23563 (2017).
24. H. Wei, E. Wang, "Nanomaterials with enzyme-like characteristics (nanozymes): Next-generation artificial enzymes," *Chem. Soc. Rev.* **42**, 6060–6093 (2013).
25. M. F. Siddiqui, Z. A. Khan, S. Park, "Detection of C-reactive protein using histag-HRP functionalized nanoconjugate with signal amplified immunoassay," *Nanomaterials* **10**, 1240 (2020).

26. R. T. K. Ariyawansha, B. F. A. Basnayake, A. K. Karunarathna, M. I. M. Mowjood, "Extensions to Michaelis–Menten kinetics for single parameters," *Sci. Rep.* **8**, 16586 (2018).
27. F. Gong, J. Chen, X. Han, J. Zhao, M. Wang, L. Feng, Y. Li, Z. Liu, L. Cheng, "Core-shell TaOx@ MnO_2 nanoparticles as a nano-radiosensitizer for effective cancer radiotherapy," *J. Mater. Chem. B* **6**, 2250–2257 (2018).
28. F. Gong, L. Cheng, N. Yang, O. Betzer, L. Feng, Q. Zhou, Y. Li, R. Chen, R. Popovtzer, Z. Liu, "Ultrasmall oxygen-deficient bimetallic oxide $MnWO_X$ nanoparticles for depletion of endogenous GSH and enhanced sonodynamic cancer therapy," *Adv. Mater.* **31**, 1900730 (2019).
29. Y. Lyu, J. Li, K. Pu, "Second near-infrared absorbing agents for photoacoustic imaging and photothermal therapy," *Small Methods* **3**, 1900553 (2019).
30. H. Tao, J. Guo, Y. Ma, Y. Zhao, T. Jin, L. Gu, Y. Dou, J. Liu, H. Hu, X. Xiong, J. Zhang, "Luminescence imaging of acute liver injury by biodegradable and biocompatible nanoprobes," *ACS Nano* **14**, 11083–11099 (2020).
31. R. Q. Yang, P. Y. Wang, K. L. Lou, Y. Y. Dang, H. N. Tian, Y. Li, Y. Y. Gao, W. H. Huang, Y. Q. Zhang, X. L. Liu, G. J. Zhang, "Biodegradable nanoprobe for NIR-II fluorescence image-guided surgery and enhanced breast cancer radiotherapy efficacy," *Adv. Sci.* **9**, 2104728 (2022).